PHYSICAL REVIEW B **88**, 104303 (2013)

Phonon polaritons in uniaxial crystals: A Raman scattering study of polaritons in α-GaN

Gert Irmer,* Christian Röder, Cameliu Himcinschi, and Jens Kortus
TU Bergakademie Freiberg, Institute of Theoretical Physics, Leipziger Str. 23, D-09599 Freiberg, Germany
(Received 31 May 2013; revised manuscript received 13 July 2013; published 12 September 2013)

We present Raman scattering results on phonon polaritons in single crystals of α-GaN. A detailed theoretical treatment of their dispersion and Raman scattering efficiency in wurtzite-type crystals is given. Pure symmetry polaritons (ordinary and extraordinary) are accessible in near-forward scattering geometry according to the theory. For this purpose, the experimental setup uses rectangular aperture windows in front of the entrance lens. Thus measurements with well defined wave-vector transfer can be realized. The observed dispersion curves and scattering efficiency results are compared with theoretical ones and are found to be in excellent agreement.

DOI: 10.1103/PhysRevB.88.104303 PACS number(s): 78.30.Fs, 31.15.es, 81.10.St

I. INTRODUCTION

In polar crystals, infrared photons strongly interact with the transverse modes of infrared active phonons if their energies are nearly equal. The elementary excitations derived are called phonon polaritons. They have mixed electromagnetic and mechanical nature and their existence has been predicted by Huang.[1,2] The frequencies of phonon polaritons occur in the terahertz (THz) spectral range. This range corresponds to the gap between high-frequency electronics and low-frequency optics. Phonon-polariton studies have recently gained interest stimulated by the generation of THz pulses by femtosecond lasers and ultrasound acoustic waves,[3] THz spectroscopy, and imaging.[4,5] Development of devices based on integrated polaritonics operating in the THz range as a potential application between integrated electronics in the microwave region and integrated optics in the near-infrared range has been discussed.[6]

Henry and Hopfield[7] were the first who observed Raman scattering of phonon polaritons in GaP in 1965. Later, phonon polaritons of several other polar semiconductors[8–12] and numerous ferroelectric crystals[13–25] have been investigated (for reviews, see Refs. 26–30) and also surface polaritons in thin films and confined structures.[31–33]

However, reports on Raman studies of phonon polaritons in uniaxial semiconductors are scarce. There is especially a lack of data on the relative intensities of the phonon polaritons. In this paper, besides discussion of general aspects of phonon polaritons for uniaxial crystals, we also derive expressions of their Raman scattering efficiency. They reflect the changing character of the phonon polaritons depending on their frequency from more photonlike to more phononlike. Contributions of the lattice displacements and the electric field associated with them to the scattering efficiency interfere constructively or destructively. Measurements of scattering efficiencies on phonon polaritons depending on frequency can be also used to determine the Faust-Henry coefficients unambiguously. These coefficients are ratios describing the relative influence of lattice displacements and electric field onto the electric susceptibility.[34–36] They are essential in order to access the charge carrier concentration as well as the mobility by Raman scattering from measured frequencies, bandwidths, and intensities of coupled phonon-plasmon modes.[36–38] A detailed discussion concerning the Faust-Henry coefficients is not the scope of this work, rather we intend to focus on novel aspects of phonon polaritons in uniaxial crystals including the discussion of Raman scattering efficiencies.

For uniaxial crystals, the conventionally used experimental setup applying annular apertures with varying diameters in front of the entrance slit of the spectrometer is meaningful only if the incident laser beam in near-forward scattering geometry is directed parallel to the c axis of the crystal and the isotropic plane coincides with the aperture plane. However, also in this case, the polaritons observed will depend on the angle and will be of mixed character. In order to observe phonon polaritons with pure symmetry, we developed a new method for near-forward scattering with a screen positioned in a plane before the first image lens which enables us to open small rectangular windows in this plane. Thus measurements with well defined wave-vector transfer can be realized. Measurements with angles down to 0.5° between the wave vectors of the exciting laser beam and the scattered light could be performed.

Besides the general interest in this material, our investigation of GaN was also stimulated by the fact that nowadays large and pure single crystals are available. GaN and its ternary alloys with Al and In are a remarkable and the most important materials system for several electronic and short-wavelength optoelectronic applications. GaN-based microelectronic devices, e.g., take advantage of the superior electronic properties for high-power, high-frequency, and high-temperature applications. Furthermore, the group-III nitride semiconductors with direct band gaps ranging from 0.7 eV (InN) through 3.4 eV (GaN) to 6.0 eV (AlN) have inspired the field of solid-state lighting. In particular, applications of these materials realizing bright, white LEDs appear very promising.[39–43]

As far as we know, only one investigation on a 70-μm-thick hexagonal GaN bulk crystal measured with near-forward scattering parallel to the c axis and annular apertures is reported by Torii *et al.*[44] However, in that work, the dependence of the Raman scattering efficiency of the polaritons on the frequency was not studied and the polaritons observed were of mixed character.

After a detailed derivation of the theoretical Raman scattering efficiency, we report on systematic measurements of ordinary and extraordinary polaritons with defined symmetry as function of the wave-vector magnitude. Moreover, it is demonstrated which range of wave vectors is attainable by Raman measurements using the experimental near-forward

scattering setup with rectangular apertures. This strongly depends on the anisotropic properties of the hexagonal crystal and can be selected by a proper polarization arrangement. The conditions which have to be fulfilled in order to detect the topmost dispersion branch (more photonlike) are discussed.

II. THEORY

A. Basic equations

According to the mixed mechanical-electromagnetic character of the phonon polaritons, we need equations of both motion and electromagnetic field. The uniaxial crystal is characterized by dielectric functions, which are identical for two principal directions:

$$\varepsilon_{11}(\omega) = \varepsilon_{22}(\omega) = \varepsilon_{\perp}(\omega). \tag{1}$$

These directions describe the optically isotropic plane. The third principal direction perpendicular to this plane is referred to as the optical axis c with the dielectric function

$$\varepsilon_{33}(\omega) = \varepsilon_{\parallel}(\omega). \tag{2}$$

The equations of motion for the polaritons will be written in a form first claimed by Huang for the description of cubic diatomic crystals with one polar mode.[1,2] In the case of a uniaxial crystal and arbitrary direction of the wave vector $\vec{k}$, the vectors $\vec{Q}$ (generalized coordinate displacement), $\vec{E}$ (electric field strength), and $\vec{P}$ (polarization) of the Born-Huang equations can be split into linearly independent "ordinary" and "extraordinary" components lying either perpendicularly to or in the plane spanned by the wave vector and the optical axis, respectively (see Fig. 1). With time dependence of the displacement vector in the form $\vec{Q} = \vec{Q}_0 e^{i\omega t}$ and without damping, we obtain for the ordinary polaritons:

$$\begin{aligned} -\omega^2 Q_{o\perp} &= B^{11}_{o\perp} Q_{o\perp} + B^{12}_{o\perp} E_{\perp}, \\ P_{o\perp} &= B^{21}_{o\perp} Q_{o\perp} + B^{22}_{o\perp} E_{\perp}, \end{aligned} \tag{3}$$

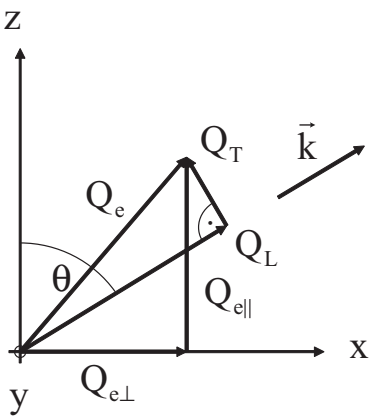

FIG. 1. Displacement components of the extraordinary polaritons, which are decomposed into parts parallel and perpendicular to the optical axis. The same procedure can be adopted for $\vec{E}$ and $\vec{P}$.

and for the extraordinary polaritons:

$$\begin{aligned} -\omega^2 Q_{e\perp} &= B^{11}_{e\perp} Q_{e\perp} + B^{12}_{e\perp} E_{\perp}, \\ P_{e\perp} &= B^{21}_{e\perp} Q_{e\perp} + B^{22}_{e\perp} E_{\perp}, \\ -\omega^2 Q_{e\parallel} &= B^{11}_{e\parallel} Q_{e\parallel} + B^{12}_{e\parallel} E_{\parallel}, \\ P_{e\parallel} &= B^{21}_{e\parallel} Q_{e\parallel} + B^{22}_{e\parallel} E_{\parallel}. \end{aligned} \tag{4}$$

As the (x,y) plane is isotropic, we will assume without loss of generality that the wave vector lies in the (x,z) plane and that the displacement of the ordinary polaritons is parallel to the y direction. The extraordinary parts of $\vec{Q}$, $\vec{E}$, and $\vec{P}$ are decomposed in components parallel and perpendicular to the z axis. This is shown in Fig. 1 for the displacement vector $\vec{Q}$ as an example.

The coefficients B can be interpreted macroscopically, and in the following sections they will be replaced by the coefficients $a_{\perp}$, $b_{\perp}$, $a_{\parallel}$, and $b_{\parallel}$ which can be expressed using measurable parameters (see Appendix A). In order to determine the nine variables in Eqs. (3) and (4) three equations are additionally needed. The relationship between the electric field $\vec{E}$ and the polarization $\vec{P}$ can be derived from Maxwell's equations. The electric displacement field $\vec{D}$ is correlated with the electric field $\vec{E}$ and the polarization $\vec{P}$ according to

$$\vec{D} = \varepsilon_o \tilde{\varepsilon} \cdot \vec{E} = \varepsilon_o \vec{E} + \vec{P}. \tag{5}$$

Here, $\tilde{\varepsilon}(\vec{k},\omega)$ refers to the dielectric tensor of the medium and ε_o denotes the permittivity. Using the ansatz of plane waves for the electric field $\vec{E} = \vec{E}_0 e^{i(\vec{k}\cdot\vec{r}-\omega t)}$ and the magnetic induction $\vec{B} = \vec{B}_0 e^{i(\vec{k}\cdot\vec{r}-\omega t)}$ and on the assumption that the medium contains neither free electrical charges ρ nor electrical currents $\vec{j}$, we obtain from Maxwell's equations

$$\vec{k} \times (\vec{k} \times \vec{E}) = \vec{k}(\vec{k} \cdot \vec{E}) - k^2 \vec{E} = -\frac{\omega^2}{c^2} \tilde{\varepsilon}\, \vec{E}. \tag{6}$$

Inserting Eq. (6) into Eq. (5), the relationship between the electric field $\vec{E}$ and the polarization $\vec{P}$ can be derived:

$$\vec{P} = \varepsilon_0 \vec{E} \left(\frac{c^2 k^2}{\omega^2} - 1 \right) - \frac{\varepsilon_0 c^2}{\omega^2} \vec{k}(\vec{k} \cdot \vec{E}). \tag{7}$$

For purely transverse waves, $\vec{E} \perp \vec{k}$, we obtain

$$\vec{P}_T = \varepsilon_0 \vec{E}_T \left(\frac{c^2 k^2}{\omega^2} - 1 \right), \tag{8}$$

and for purely longitudinal waves, $\vec{E} \parallel \vec{k}$, we obtain

$$\vec{P}_L = -\varepsilon_0 \vec{E}_L. \tag{9}$$

$\omega_{T\perp}$ ($\omega_{T\parallel}$) indicates the frequency of the transverse phonon propagating in the (x,y) plane (parallel to the z axis). $\omega_{L\perp}$ ($\omega_{L\parallel}$) refers to the frequency of the longitudinal phonon propagating in the (x,y) plane (parallel to the z axis). $\varepsilon_{s\perp}$ ($\varepsilon_{\infty\perp}$) denotes the static (high-frequency) dielectric constant in the (x,y) plane and $\varepsilon_{s\parallel}$ ($\varepsilon_{\infty\parallel}$) the static (high-frequency) dielectric constant parallel to the z axis.

The numerical calculations in the next sections are based on hexagonal α-GaN with parameters given in Sec. III B. The primitive unit cell of α-GaN with space group C^4_{6v} contains four atoms. One Ga atom of the two GaN pairs is tetrahedrally coordinated by four N atoms, and vice versa. Group theory

predicts $3 \times 4 = 12$ phonon normal modes at the Γ point of the Brillouin zone according to the irreducible representation $2A_1 + 2B_1 + 2E_1 + 2E_2$. One set of A_1 and E_1 modes are acoustic, while the remaining $A_1 + 2B_1 + E_1 + 2E_2$ modes are optical ones. The A_1 and E_1 modes are both Raman and IR (infrared) active, the two E_2 modes are only Raman active, and the two B_1 modes are silent modes (neither Raman nor IR active). Only the polar A_1 and E_1 modes show polariton dispersion. They split into TO and LO phonon modes with different frequencies due to the macroscopic electric field associated with the longitudinal modes. In the case of GaN, the electrostatic forces predominate over the anisotropic short-range forces. Therefore the TO-LO splitting is larger than the A_1-E_1 splitting.[45] For the lattice vibrations with A_1 and E_1 symmetry, the atomic displacement is parallel and perpendicular to the c axis, respectively. Thus phonons with wave-vector angles between 0° and 90° to the c axis have mixed A_1-E_1 character.

B. Ordinary polaritons

In order to solve the three equations Eqs. (3) and (8), we combine $Q_{o\perp}$, $E_{o\perp}$, and $P_{o\perp}$ to a vector $\vec{X}_o$. The set of equations can then be written as

$$\tilde{M}_o \cdot \vec{X}_o = 0 \tag{10}$$

with the matrix

$$\tilde{M}_o = \begin{pmatrix} \omega^2 - \omega_{T\perp}^2 & a_\perp & 0 \\ a_\perp & b_\perp & -1 \\ 0 & \varepsilon_0\left(\frac{c^2k^2}{\omega^2} - 1\right) & -1 \end{pmatrix}.$$

Nontrivial solutions of the equations are obtained with $\det(\tilde{M}_o) = 0$. This leads to the equation

$$\varepsilon_{\infty\perp}\omega^4 - \omega^2c^2k^2 - \varepsilon_{\infty\perp}\omega^2\omega_{L\perp}^2 + c^2k^2\omega_{T\perp}^2 = 0. \tag{11}$$

This equation can also be written as

$$\frac{c^2k^2}{\omega^2} = \varepsilon_\perp(\omega) = \varepsilon_{\infty\perp}\left(1 + \frac{\omega_{L\perp}^2 - \omega_{T\perp}^2}{\omega_{T\perp}^2 - \omega^2}\right), \tag{12}$$

where $\varepsilon_\perp(\omega)$ is the dielectric function for propagation in the optically isotropic plane. Equation (11) is a quadratic equation in ω^2. Its solution gives two polariton branches that do not depend on the angle θ. For $k \to 0$, the lower branch converges to zero and the upper to the frequency of the LO(E_1) phonon mode. For large k, the lower branch reaches the frequency of the transverse phonon TO(E_1) (see Fig. 2).

C. Extraordinary polaritons

It is convenient to change the coordinate system and express the vectors $\vec{Q}$, $\vec{E}$, and $\vec{P}$ in components parallel (L*ongitudinal*) and perpendicular (T*ransverse*) to the wave vector $\vec{k}$ (see Fig. 1). Thus the polarization can be easily expressed by components parallel to the corresponding electric field components [see Eqs. (8) and (9)]. In order to solve six equations (4), (8), and (9), we combine the transformed components $Q_{e\perp}$, $E_{e\perp}$, $P_{e\perp}$, $Q_{e\parallel}$, $E_{e\parallel}$, and $P_{e\parallel}$ to a vector $\vec{X}_e$ and write the set of equations in the form

$$\tilde{M}_e \cdot \vec{X}_e = 0 \tag{13}$$

with the matrix

$$\tilde{M}_e = \begin{pmatrix} -\left(\omega^2 - \omega_{T\perp}^2\right)\cos\theta & -a_\perp\cos\theta & 0 & \left(\omega^2 - \omega_{T\perp}^2\right)\sin\theta & a_\perp\sin\theta & 0 \\ -a_\perp\cos\theta & -b_\perp\cos\theta & \cos\theta & a_\perp\sin\theta & b_\perp\sin\theta & -\sin\theta \\ 0 & \varepsilon_0\left(1 - \frac{c^2k^2}{\omega^2}\right) & 1 & 0 & 0 & 0 \\ \left(\omega^2 - \omega_{T\parallel}^2\right)\sin\theta & a_\parallel\sin\theta & 0 & \left(\omega^2 - \omega_{T\parallel}^2\right)\cos\theta & a_\parallel\cos\theta & 0 \\ a_\parallel\sin\theta & b_\parallel\sin\theta & -\sin\theta & a_\parallel\cos\theta & b_\parallel\cos\theta & -\cos\theta \\ 0 & 0 & 0 & 0 & \varepsilon_0 & 1 \end{pmatrix}.$$

Nontrivial solutions of this homogeneous equation system for the six variables Q_T, E_T, P_T, Q_L, E_L, and P_L are obtained for vanishing determinant $\tilde{M}_e$. This leads to the equation

$$\left(\frac{c^2k^2}{\omega^2}\right)[\varepsilon_\perp(\omega)\,\sin^2\theta + \varepsilon_\parallel(\omega)\,\cos^2\theta] - \varepsilon_\perp(\omega)\,\varepsilon_\parallel(\omega) = 0, \tag{14}$$

where $\varepsilon_\perp(\omega)$ and $\varepsilon_\parallel(\omega)$ are the dielectric functions for propagation in the optically isotropic plane and parallel to the c axis of the uniaxial crystal, respectively. $\varepsilon_\perp(\omega)$ is given by Eq. (12) and $\varepsilon_\parallel(\omega)$ is defined by

$$\varepsilon_\parallel(\omega) = \varepsilon_{\infty\parallel}\left(1 + \frac{\omega_{L\parallel}^2 - \omega_{T\parallel}^2}{\omega_{T\parallel}^2 - \omega^2}\right). \tag{15}$$

Equation (14) describes the directional dispersion as well as the dispersion as a function of the wave vector. This equation is cubic in ω^2 and can be solved analytically using Cardano' s formula.[46] The three real solutions describe the three branches of the extraordinary polaritons. [Conventionally, the notation polariton is restricted to the transverse polariton branches with their strong frequency dependence. On the contrary, the changes in the LO frequencies are minor. However, for small wave vectors ($k < 5 \times 10^3$ cm^{-1}) interaction between phonon and photon can be seen (see Fig. 3). Therefore, in this work, we use the notation polariton for all branches which are solutions of Eq. (14).] In the following, we discuss $\omega(\vec{k})$ in dependence on the angle θ between the wave vector and the z axis.

a. $\theta = 0^\circ$. The low branch converges for $k \to 0$ to zero and the high branch to ω_{E_1LO}. From the solution $\varepsilon_\parallel(\omega) = 0$, the

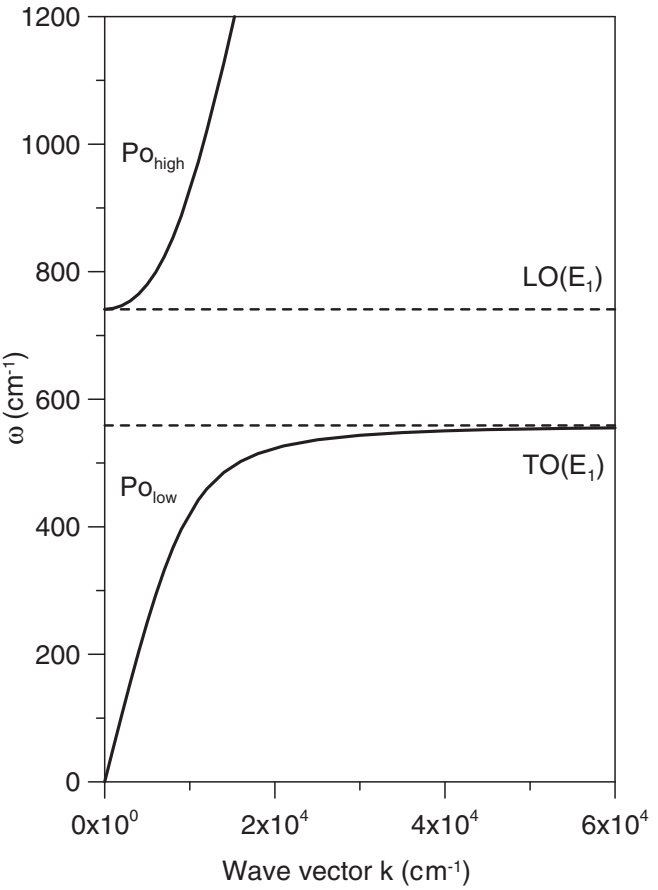

FIG. 2. Solutions of Eq. (11): dispersion of the phononlike $PO_{o,low}$ and the photonlike $PO_{o,high}$ branches of the ordinary polariton in α-GaN (E_1 type) as a function of the wave vector k.

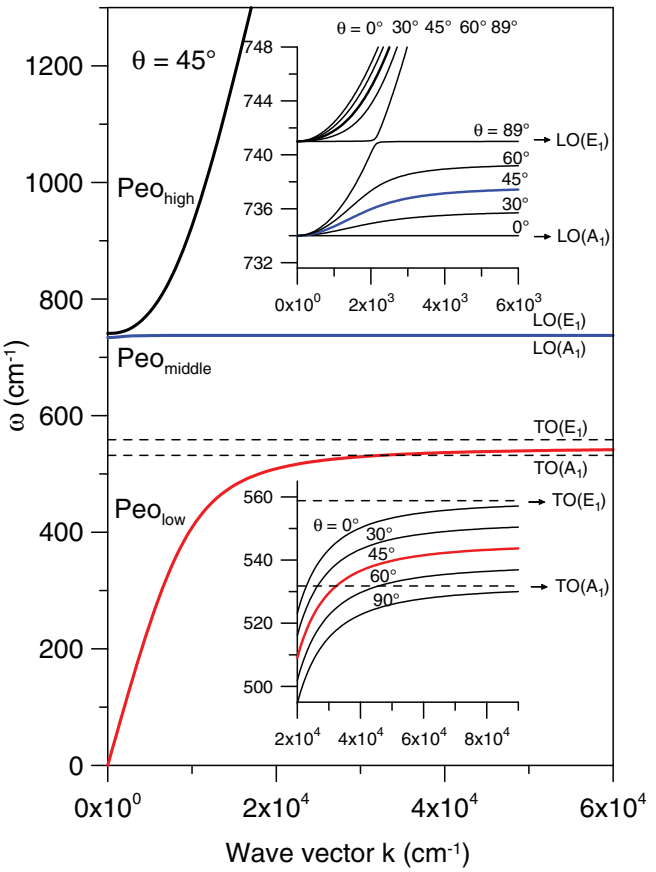

FIG. 3. (Color online) Solutions of Eq. (14): dispersion of the TO-phonon-like $PO_{eo,low}$, the LO-phonon-like $PO_{eo,middle}$, and the photonlike $PO_{eo,high}$ extraordinary polariton branches in α-GaN in dependence on the wave vector k for a fixed angle $\theta = 45°$ between the wave vector and the z axis. The insets show the dispersion of the extraordinary polariton branches for small wave vectors in dependence on the angle θ.

$LO(A_1)$ phonon is obtained with $\omega = \omega_{L\parallel}$. The other solutions describe the extraordinary transverse polaritons associated with polaritons of E_1 type with displacements parallel to the c axis. These branches coincide with the directionally independent ordinary polariton of E_1 type (see Fig. 2). The frequency of the middle branch is independent on k. For large k, the low branch reaches ω_{E_1TO}.

b. $\theta = 90°$. The low branch converges for $k \to 0$ to zero and the high branch to ω_{E_1LO}. The frequency of the middle branch corresponds to ω_{E_1LO} and is independent on k. Since the polariton is of A_1 type for large k the low branch reaches ω_{A_1TO}.

c. $0° < \theta < 90°$. For $k \to 0$ the low branch reaches zero and the high branch ω_{E_1LO}. The middle branch shows dispersion depending on the value k with frequencies ranging between ω_{A_1LO} and ω_{E_1LO}. The low branch converges for large k to a frequency value between ω_{A_1TO} and ω_{E_1TO}. The frequency limits for $k \to \infty$ can be calculated for the low and the middle branches using Eq. (14). As an example, Fig. 3 shows the extraordinary polaritons for $\theta = 45°$ and in the insets for other angles θ as well. For $k \to 0$, the polaritons are independent on the angle θ of the wave vector with the c axis and approach the limiting frequencies 0, ω_{A_1LO} and ω_{E_1LO}. From a physical point of view, if the wavelength approaches infinity, then the lattice vibrations cease to sense the wave vector direction. The lattice displacements and associated electric fields are parallel or perpendicular to the c axis.

D. Directional dispersion

For large wave vectors (10^4 cm$^{-1} < k < 10^6$ cm^{-1}), the polaritons are phononlike. Assuming $k \to \infty$, we obtain from Eq. (14):

$$\varepsilon_\perp(\omega)\,\sin^2\theta + \varepsilon_\parallel(\omega)\,\cos^2\theta = 0. \tag{16}$$

The solution of this quadratic equation in ω^2 yields two extraordinary polariton (phonon) branches depending on the angle θ including the wave vector and the c axis of the crystal. The directional dispersion of the two extraordinary modes is shown in Fig. 4. The ordinary phonon of E_1 symmetry and TO character exhibits no dispersion. For comparison, the nonpolar mode $E_{2,high}$ is shown which also has no directional dispersion.

In order to describe the directional dependence, the Poulet-Loudon approximation[47,48] is a simple expression used in the literature:

$$\begin{aligned}\omega^2_{TO}(\theta) &= \omega^2_{E_1TO}\,\cos^2\theta + \omega^2_{A_1TO}\,\sin^2\theta,\\ \omega^2_{LO}(\theta) &= \omega^2_{A_1LO}\,\cos^2\theta + \omega^2_{E_1LO}\,\sin^2\theta.\end{aligned} \tag{17}$$

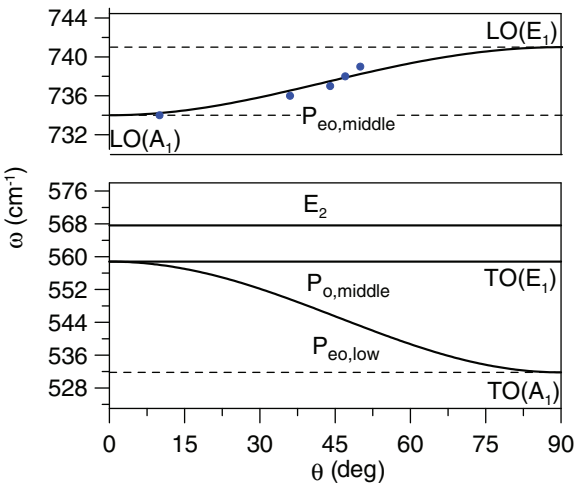

FIG. 4. (Color online) Solutions of Eq. (14) in the case of large wave vectors: directional dispersion of the extraordinary TO phonons and LO phonons in α-GaN. The circles in the upper part of the figure show measured frequencies of the LO phonon (see Sec. IV, Fig. 7).

In the case of α-GaN, these approximations work very well and practically coincide with the exact solutions shown in Fig. 4. The circles in the upper part of the figure present measured frequencies of the LO phonon taken from near-forward scattering in the (x,z) plane (see Sec. IV).

E. Raman scattering intensity

The Raman scattering efficiency per unit angle $\frac{\mathrm{d}S}{\mathrm{d}\Omega}$ of the polaritons traveling the distance L in the crystal through the volume V can be written[29] as

$$\frac{\mathrm{d}S}{\mathrm{d}\Omega} = \left(\frac{\omega_\mathrm{s}}{c}\right)^4 VL \left| \langle 1+n_\omega | \sum_{\mu\nu=1}^{3} e^\mathrm{S}_\mu \delta\chi_{\mu\nu} e^\mathrm{L}_\nu | n_\omega \rangle \right|^2, \quad (18)$$

where $\vec{e}^\mathrm{L}(\vec{e}^\mathrm{S})$ are the unit vectors in direction of polarization of the incident (scattered) photons, respectively. The value inside the absolute value signs is the matrix element of an operator between the state with n_ω polaritons of frequency ω present and the state with $n_\omega + 1$ polaritons describing a Stokes scattering process. $n_\omega = 1/[\exp(\hbar\omega/kT) - 1]$ is the Bose-Einstein factor. The Raman scattering intensity depends on the changes $\delta\chi$ of the polarizability tensor with contributions of the normal coordinates and the electric field components:

$$\begin{aligned}
\delta\chi^N &= \frac{\partial\chi}{\partial Q_N} Q_N + \frac{\partial\chi}{\partial E_N} E_N \\
&= \left[\frac{\partial\chi}{\partial Q_N} + \frac{(\omega^2_{\mathrm{T}N} - \omega^2)}{\omega_{\mathrm{T}N}\sqrt{\varepsilon_0(\varepsilon_{\mathrm{s}N} - \varepsilon_{\infty N})}} \frac{\partial\chi}{\partial E_N} \right] Q_N \\
&= \left\{ \sum_{\alpha=1}^{3} \left[\frac{\partial\chi}{\partial Q_\alpha}\frac{\partial Q_\alpha}{\partial Q_N} + \frac{(\omega^2_{\mathrm{T}N} - \omega^2)}{\omega_{\mathrm{T}N}\sqrt{\varepsilon_0(\varepsilon_{\mathrm{s}N} - \varepsilon_{\infty N})}} \right.\right. \\
&\quad \left.\left. \times \frac{\partial\chi}{\partial E_\alpha}\frac{\partial E_\alpha}{\partial E_N} \right] \right\} Q_N, \\
&\quad \text{for} \quad N = 1,2, \quad \omega_N = \omega_{\mathrm{T}\perp}, \\
&\quad \text{for} \quad N = 3, \quad \omega_N = \omega_{\mathrm{T}\parallel}. \qquad (19)
\end{aligned}$$

The letter N denotes the ordinary transverse, extraordinary transverse, and the extraordinary longitudinal polaritons with the normal coordinates Q_To, Q_Te, Q_Le and the electric fields E_To, E_Te, E_Le, respectively. The relation between E_N and Q_N follows from Eqs. (3) and (4).

We decompose the normal coordinates introducing the angles φ and θ, which define the direction of the wave vector $\vec{k} = k\ (\sin\theta\cos\varphi,\ \sin\theta\sin\varphi,\ \cos\theta)$. The direction of the three normal coordinates $\vec{Q}_\mathrm{To} \perp \vec{Q}_\mathrm{Te} \perp \vec{Q}_\mathrm{Le}$ is given by $\vec{Q}_\mathrm{To} \perp (z$ axis, $\vec{k})$, $\vec{Q}_\mathrm{Te} \perp (\vec{k},\ \vec{Q}_\mathrm{To})$, and $\vec{Q}_\mathrm{Le} \parallel \vec{k}$. We obtain

$$\begin{aligned}
\frac{\partial\chi}{\partial Q_\mathrm{To}} &= \frac{\partial\chi}{\partial Q_x}\frac{\partial Q_x}{\partial Q_\mathrm{To}} + \frac{\partial\chi}{\partial Q_y}\frac{\partial Q_y}{\partial Q_\mathrm{To}} + \frac{\partial\chi}{\partial Q_z}\frac{\partial Q_z}{\partial Q_\mathrm{To}} \\
&= -\frac{\partial\chi}{\partial Q_x}\sin\varphi + \frac{\partial\chi}{\partial Q_y}\cos\varphi, \\
\frac{\partial\chi}{\partial Q_\mathrm{Te}} &= \frac{\partial\chi}{\partial Q_x}\frac{\partial Q_x}{\partial Q_\mathrm{Te}} + \frac{\partial\chi}{\partial Q_y}\frac{\partial Q_y}{\partial Q_\mathrm{Te}} + \frac{\partial\chi}{\partial Q_z}\frac{\partial Q_z}{\partial Q_\mathrm{Te}} \\
&= -\frac{\partial\chi}{\partial Q_x}\cos\theta\cos\varphi - \frac{\partial\chi}{\partial Q_y}\cos\theta\sin\varphi + \frac{\partial\chi}{\partial Q_z}\sin\theta, \\
\frac{\partial\chi}{\partial Q_\mathrm{Le}} &= \frac{\partial\chi}{\partial Q_x}\frac{\partial Q_x}{\partial Q_\mathrm{Le}} + \frac{\partial\chi}{\partial Q_y}\frac{\partial Q_y}{\partial Q_\mathrm{Le}} + \frac{\partial\chi}{\partial Q_z}\frac{\partial Q_z}{\partial Q_\mathrm{Le}} \\
&= \frac{\partial\chi}{\partial Q_x}\sin\theta\cos\varphi + \frac{\partial\chi}{\partial Q_y}\sin\theta\sin\varphi + \frac{\partial\chi}{\partial Q_z}\cos\theta. \qquad (20)
\end{aligned}$$

Similarly, the components of the electro-optic tensor are obtained.

We use the abbreviations $a_{\alpha,ij} = \frac{\partial\chi_{ij}}{\partial Q_\alpha}$ for the coefficients of the atomic displacement tensor and $b_{\alpha,ij} = \frac{\partial\chi_{ij}}{\partial E_\alpha}$ for the coefficients of the electro-optic tensor. The coefficients of the electro-optic tensor are related to those of the second harmonic generation tensor $d_{\alpha,ij}$:[49]

$$b_{\alpha,ij} = 4\, d_{\alpha,ij}. \qquad (21)$$

Tables for the Raman tensors have been published by several authors. We refer to the table in Claus *et al.*[30] where some errors appearing in older tables have been corrected. For the polar modes in hexagonal crystals with point group C_{6v}, the tensors have the following form:

$$\alpha = 1, \quad E_1(x): \quad \frac{\partial\chi}{\partial Q_x} = \begin{pmatrix} 0 & 0 & c_\mathrm{Q} \\ 0 & 0 & 0 \\ c_\mathrm{Q} & 0 & 0 \end{pmatrix}, \quad \frac{\partial\chi}{\partial E_x} = \begin{pmatrix} 0 & 0 & c_\mathrm{e} \\ 0 & 0 & 0 \\ c_\mathrm{e} & 0 & 0 \end{pmatrix},$$

$$\alpha = 2, \quad E_1(y): \quad \frac{\partial\chi}{\partial Q_y} = \begin{pmatrix} 0 & 0 & 0 \\ 0 & 0 & c_\mathrm{Q} \\ 0 & c_\mathrm{Q} & 0 \end{pmatrix}, \quad \frac{\partial\chi}{\partial E_y} = \begin{pmatrix} 0 & 0 & 0 \\ 0 & 0 & c_\mathrm{e} \\ 0 & c_\mathrm{e} & 0 \end{pmatrix},$$

$$\alpha = 3, \quad A_1(z): \ \frac{\partial \chi}{\partial Q_z} = \begin{pmatrix} a & 0 & 0 \\ 0 & a & 0 \\ 0 & 0 & b \end{pmatrix},$$
$$\frac{\partial \chi}{\partial E_z} = \begin{pmatrix} a_e & 0 & 0 \\ 0 & a_e & 0 \\ 0 & 0 & b_e \end{pmatrix}. \quad (22)$$

We have written c_Q to avoid confusion with the velocity of light c.

We express the relation between the electro-optic tensor components and the atomic displacement tensor components using the Faust-Henry[34] coefficients:

$$b_{\alpha,ij} = \frac{a_{\alpha,ij}\sqrt{\varepsilon_0(\varepsilon_{s\alpha} - \varepsilon_{\infty\alpha})}}{C^{FH}_{\alpha,ij}\ \omega_{T\alpha}}. \quad (23)$$

According to the symmetry of the tensors, three different Faust-Henry coefficients will appear:

$$C^{FH}_c = C^{FH}_{1,31} = C^{FH}_{1,13} = C^{FH}_{2,23} = C^{FH}_{2,32},$$
$$C^{FH}_a = C^{FH}_{3,11} = C^{FH}_{3,22}, \quad (24)$$
$$C^{FH}_b = C^{FH}_{3,33}.$$

The Faust-Henry coefficients can be obtained by measurement of the Raman scattering intensities I_{LO} and I_{TO} of the corresponding LO and TO phonons:

$$\frac{I_{LO}}{I_{TO}} = \frac{\omega_{TO}}{\omega_{LO}} \frac{n(\omega_{LO}) + 1}{n(\omega_{TO}) + 1} \left| 1 - \frac{\omega^2_{LO} - \omega^2_{TO}}{C^{FH}\omega^2_{TO}} \right|^2. \quad (25)$$

The Raman scattering intensity can now be written as

$$I_N(\omega) = \left(\frac{\omega_s}{c}\right)^4 V L |\vec{e}^L \cdot \tilde{R}_N \cdot \vec{e}^S|^2 |\langle 1 + n_\omega | Q_N | n_\omega \rangle|^2. \quad (26)$$

The index N refers to ordinary transverse polaritons (N = To), extraordinary transverse polaritons (N = Te), or extraordinary longitudinal polaritons (N = Le), respectively. The three matrices $\tilde{R}_N$ are

$$\tilde{R}_{To} = C \cdot \begin{pmatrix} 0 & 0 & -\sin\varphi \\ 0 & 0 & \cos\varphi \\ -\sin\varphi & \cos\varphi & 0 \end{pmatrix} \quad (27)$$

with $C(\omega) = c_Q(1 + \frac{\omega^2_{T\perp} - \omega^2}{C^{FH}_c \omega^2_{T\perp}})$,

$$\tilde{R}_{Te} = \begin{pmatrix} A\sin\theta & 0 & -C\cos\theta\cos\varphi \\ 0 & A\sin\theta & -C\cos\theta\sin\varphi \\ -C\cos\theta\cos\varphi & -C\cos\theta\sin\varphi & B\sin\theta \end{pmatrix} \quad (28)$$

and

$$\tilde{R}_{Le} = \begin{pmatrix} A\cos\theta & 0 & C\sin\theta\cos\varphi \\ 0 & A\cos\theta & C\sin\theta\sin\varphi \\ C\sin\theta\cos\varphi & C\sin\theta\sin\varphi & B\cos\theta \end{pmatrix} \quad (29)$$

with $A(\omega) = a(1 + \frac{\omega^2_{T\parallel} - \omega^2}{C^{FH}_a \omega^2_{T\parallel}})$ and $B(\omega) = b(1 + \frac{\omega^2_{T\parallel} - \omega^2}{C^{FH}_b \omega^2_{T\parallel}})$.

Matrix elements $|\langle 1 + n_\omega | Q_N | n_\omega \rangle|^2$ have been calculated for polar modes in cubic crystals by Mills and Burstein[29] introducing a so-called phonon strength function with electromagnetic and mechanical contributions to the polaritons energy. However, generalizing for uniaxial crystals, the calculation of the matrix elements leads to the following:

$$|\langle 1 + n_\omega | Q_{To} | n_\omega \rangle|^2 = \left[\frac{\hbar(1 + n_\omega)}{2V\omega_{T\perp}}\right] S_{p\perp},$$
$$|\langle 1 + n_\omega | Q_{Te} | n_\omega \rangle|^2 = \left[\frac{\hbar(1 + n_\omega)}{2V}\right] \times \left(\frac{S_{p\perp}\cos^2\theta}{\omega^2_{T\perp}} + \frac{S_{p\parallel}\sin^2\theta}{\omega^2_{T\parallel}}\right),$$
$$|\langle 1 + n_\omega | Q_{Le} | n_\omega \rangle|^2 = \left[\frac{\hbar(1 + n_\omega)}{2V}\right] \times \left(\frac{S_{p\perp}\sin^2\theta}{\omega^2_{T\perp}} + \frac{S_{p\parallel}\cos^2\theta}{\omega^2_{T\parallel}}\right), \quad (30)$$

with

$$S_{p\perp}(\omega) = \frac{\omega\omega_{T\perp}(\omega^2_{L\perp} - \omega^2_{T\perp})}{(\omega^2_{T\perp} - \omega^2) + \omega^2_{T\perp}(\omega^2_{L\perp} - \omega^2_{To\perp})},$$
$$S_{p\parallel}(\omega) = \frac{\omega\omega_{T\parallel}(\omega^2_{L\parallel} - \omega^2_{T\parallel})}{(\omega^2_{T\parallel} - \omega^2) + \omega^2_{T\parallel}(\omega^2_{L\parallel} - \omega^2_{T\parallel})}. \quad (31)$$

The phonon strength functions $S_{p\perp}(\omega)$ and $S_{p\parallel}(\omega)$ provide a measure of the phonon content of the polaritons depending on their frequency. If the frequencies of the transverse polaritons approach the phonon frequencies ($\omega \to \omega_{T\perp}$ and $\omega \to \omega_{T\parallel}$) in case of large wave vectors, the phonon strength functions approach unity. For the longitudinal polaritons with $\omega \to \omega_{L\perp}$ ($\omega \to \omega_{L\parallel}$), we obtain $S_{p\perp} = \omega_{T\perp}/\omega_{L\perp}$ ($S_{p\parallel} = \omega_{T\parallel}/\omega_{L\parallel}$). Equation (26) describes the Raman scattering intensity of the polaritons (near-forward scattering) as well as of the phonons (180°-backscattering or 90°-scattering geometry).

III. EXPERIMENT

A. Near-forward scattering

The scattering configuration is shown in Fig. 5. The exciting laser beam is directed along the x axis and enters the entrance surface of the prismatic sample. The screen placed directly in front of the entrance lens of the imaging system is open for scattered light with a small window around the point (Y, Z). The scattered light beam includes the angle ψ with the (x, y) plane, and its orthogonal projection on the (x, y) plane the angle δ with the x axis. Afterwards, the scattered light originating from the focus plane of the entrance lens passes an analyzer and a quartz wave plate, which rotates the polarization axis in the position for which the spectrometer throughput is optimized.

For the scattering process inside the crystal [see Fig. 5(b) and 5(c), index "i"] wave-vector conservation requires

$$\vec{k}_{iL} = \vec{k}_{iS} + \vec{k}_P \quad (32)$$

and energy conservation requires

$$\hbar\omega_L = \hbar\omega_S + \hbar\omega_P \quad \text{or} \quad \frac{1}{\lambda_L} = \frac{1}{\lambda_S} + \omega. \quad (33)$$

The laser wave-vector magnitude is $|\vec{k}_{iL}| = \frac{2\pi n_L}{\lambda_L}$ and the magnitude of the scattered light wave vector is $|\vec{k}_{iS}| = \frac{2\pi n_S}{\lambda_S}$. λ_L and λ_S denote the wavelength of the incident and scattered

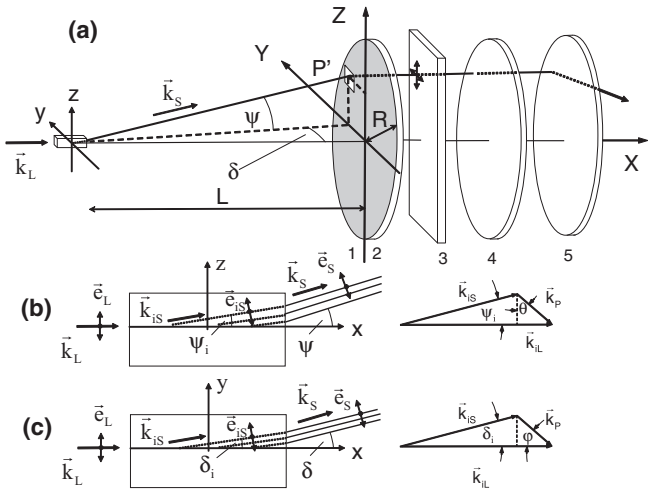

FIG. 5. Setup for near-forward scattering: (a) scattered light with wave vector $\vec{k}_S$ outside the crystal enters the window P' at (Y,Z) on the masking screen (1) positioned in front of the lens (2), passes the analyzer (3), $\lambda/2$ quartz wave plate (4) and lens (5). Introducing spherical coordinates, the scattered light beam includes the angle ψ with the (x,y) plane and the azimuthal angle δ. Refraction at the crystal boundary: (b) special case: scattering in the (x,z) plane. The wave vector $\vec{k}_S$ of the scattered light (angle ψ with the x axis) corresponds to the wave vector $\vec{k}_{iS}$ with the angle ψ_i inside the crystal. (c) Special case: scattering in the (x,y) plane. The wave vector $\vec{k}_S$ of the scattered light (angle δ with the x axis) corresponds to the wave vector $\vec{k}_{iS}$ with the angle δ_i inside the crystal.

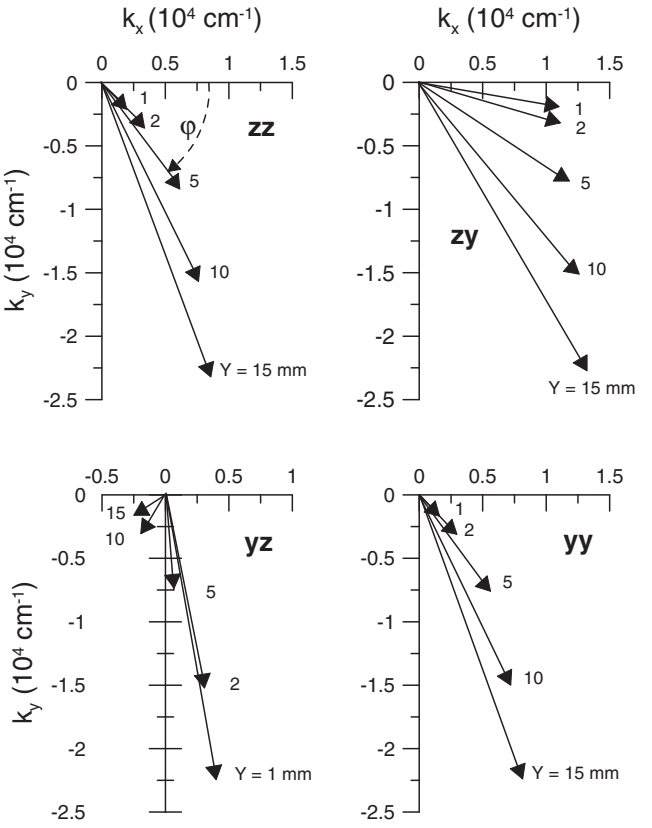

FIG. 6. Polariton wave vectors for near-forward scattering in direction x in the (x,y) plane. The wave vector of the scattered light is directed to the window at Y (and for $Z=0$) on the masking screen (see Fig. 5). The two letters indicate the polarization direction of the incident and scattered light, respectively.

photons outside the crystal, respectively. $\vec{k}_P$ refers to the wave vector of the polariton excited in a Stokes process and ω to its energy expressed in cm^{-1}. Since α-GaN is a uniaxial crystal, we have to differentiate between ordinary and extraordinary rays of the incident and scattered light. The refraction indices n_L and n_S are used for ordinary (extraordinary) rays. For ordinary rays, the electric field is polarized in the (x,y) plane. The proper refractive index is $n_o = \sqrt{\varepsilon_{\infty\perp}}$. For extraordinary rays, the electric field is polarized parallel to the z axis and the corresponding refractive index can be expressed by $n_{eo} = \sqrt{\varepsilon_{\infty\parallel}}$. $\varepsilon_{\infty\perp}$ indicates the high-frequency dielectric constant in the (x,y) plane and $\varepsilon_{\infty\parallel}$ for directions parallel to the z axis. We consider near-forward scattering with the c axis of the crystal oriented parallel to the z axis of the laboratory coordinate system and the scattering geometries $x(zz)x$, $x(zy)x$, $x(yz)x$, and $x(yy)x$. The letters in brackets describe the polarization direction of the incident and scattered light beam, respectively.

Light scattered inside the crystal with wave vector $\vec{k}_{iS}$ enters the small window on the screen located at $(Y,Z) = (L\tan\delta, L\tan\psi)$ with wave vector $\vec{k}_S$. The vectors $\vec{k}_{iS}$, $\vec{k}_P$, and $\vec{e}_{iS}$ characterising the scattering process inside the crystal can be expressed as functions of the window position (angles ψ and δ). Details are shown in Appendix B. For the wave vector $\vec{k}_{iS}$ of scattered light inside the crystal, we obtain

$$\vec{k}_{iS} = \frac{2\pi n_S}{\lambda_S}\left(\sqrt{1-a}, \frac{-\sqrt{a}}{\sqrt{1+b}}, \frac{\sqrt{ab}}{\sqrt{1+b}}\right), \qquad (34)$$

where $a = (1-\cos^2\psi\cos^2\delta)/n_S^2$ and $b = (\tan^2\psi/\sin^2\delta)/n_S^2$. Depending on the polarization, the refractive index rates as $n_S = n_o$ (ordinary ray) or $n_S = n_{eo}$ (extraordinary ray). The polariton wave vector $\vec{k}_P$ is obtained using Eq. (32). For the polarization configuration (yz) the component $k_{P,x}$ can also be negative (see Fig. 6).

B. Experimental conditions

Raman spectra were obtained at room temperature using a T 64000 Raman spectrometer (Horiba, Jobin Yvon) in a nearly forward scattering geometry. For this purpose, the GaN sample was positioned in the macrochamber with its c axis oriented parallel to the z axis of the laboratory coordinate system. The spectra were excited applying the 514.5-nm line of an Ar^+ laser at a power level of about 100 mW at the sample. After passing the spectrometer equipped with gratings of 1800 grooves/mm in subtractive mode, the scattered light was detected by a LN cooled CCD detector. The laser beam was focused onto the sample by a laser objective. By means of a polarization rotator, the laser beam polarization could be changed from (i) parallel to the y axis (H) with the ordinary ray inside the crystal to (ii) parallel to the z axis (V) with extraordinary ray inside the crystal (see Fig. 5). The scattered light was analyzed with polarization parallel or perpendicular to the z axis using an analyzer positioned in the parallel light path between sample and entrance slit of the spectrometer. Both laser beam and sample were carefully adjusted in order to avoid the capture of laser light into the spectrometer. The laser beam leaving

the sample was masked in the center of the entrance lens of the imaging system. Furthermore, care is necessary to avoid gathering of scattered light excited by the laser beam partly backscattered at the inner crystal surface. The reflectivity at 514.5-nm wavelength is about 0.174 (0.157) for the ordinary (extraordinary) beam.[50]

Since there is an excellent agreement with our experimental data the following parameters were adopted in this work and used for the calculations: $\varepsilon_o = 5.20\ \mathrm{cm}^{-1}$, $\varepsilon_{eo} = 5.31\ \mathrm{cm}^{-1}$;[51] $\omega_{A_1TO} = 531.8\ \mathrm{cm}^{-1}$, $\omega_{E_1TO} = 558.8\ \mathrm{cm}^{-1}$, $\omega_{E_2high} = 567.6\ \mathrm{cm}^{-1}$, $\omega_{E_2low} = 144\ \mathrm{cm}^{-1}$, $\omega_{A_1LO} = 734\ \mathrm{cm}^{-1}$, and $\omega_{E_1LO} = 741\ \mathrm{cm}^{-1}$.[52]

IV. EXPERIMENTAL RESULTS

Although the birefringence of α-GaN is only weak ($n_o = \sqrt{\varepsilon_{\infty\perp}} = 2.280, n_e = \sqrt{\varepsilon_{\infty\parallel}} = 2.304$),[51] its optical anisotropy has a strong impact on the polariton spectra measured with different polarizations of the incident and scattered light. Figure 6 shows transferred polariton wave vectors for scattering in the (x,y) plane for the near-forward scattering configurations $x(zz)x$, $x(yy)x$, $x(zy)x$, and $x(yz)x$. The parameter Y describes the position of the opened window in horizontal direction ($Z = 0$) on the screen in front of the entrance lens. Note the strong difference between the polarizations (zy) and (yz) for hexagonal α-GaN. In the case of cubic β-GaN, however, the polariton wave vectors and the Raman spectra of the two polarizations should be the same. The ordinary ($\vec{e}_L \parallel y$) or extraordinary ($\vec{e}_L \parallel z$) laser light propagates inside the crystal along the x axis. The outgoing scattered light is extraordinary ($\vec{e}_S \parallel z$) or ordinary ($\vec{e}_S \parallel y$). The extraordinary polaritons are observable with (zz) or (yy) polarizations, whereas the ordinary ones can be detected in (zy) or (yz) polarization configuration.

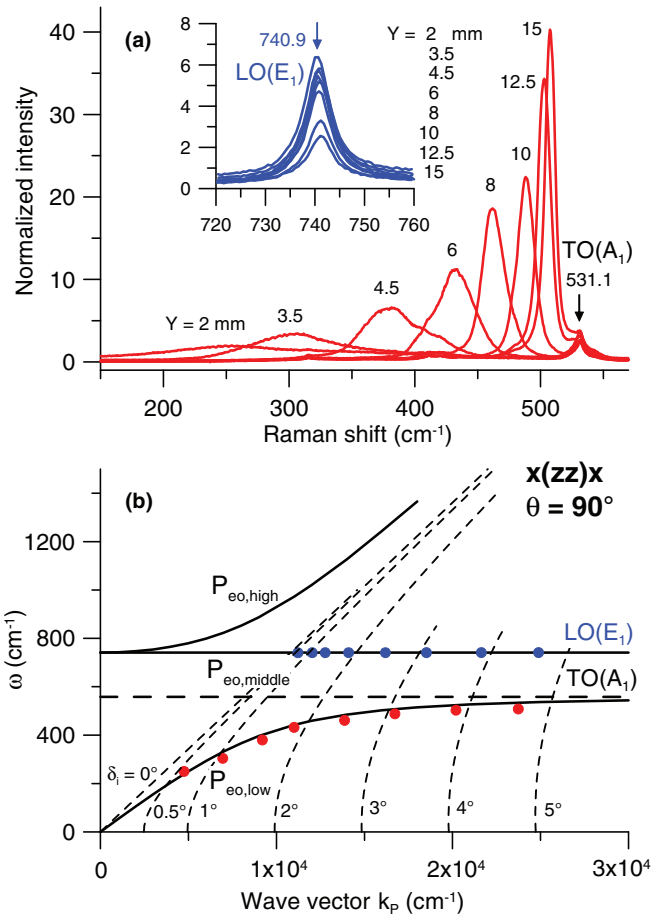

FIG. 7. (Color online) (a) Raman spectra of the extraordinary polariton, $\theta = 90^\circ$, $x(zz)x$. Near-forward scattering in direction x, scattering in the (x,y) plane, polarization parallel $z(z)$ of the incident (scattered) light vectors. The parameter Y indicates the position of the entrance window for the scattered light on the screen (1), Z =0. The inset shows the LO(E_1) phonon at fixed spectral position. (b) Dispersion of the extraordinary polariton branches for $\theta = 90^\circ$ as a function of the polariton wave vector [solutions of Eq. (14)]. The dashed curves [solutions of Eq. (B2)] show possible (ω, k_P) values for scattering angles δ_i inside the crystal (see Fig. 5).

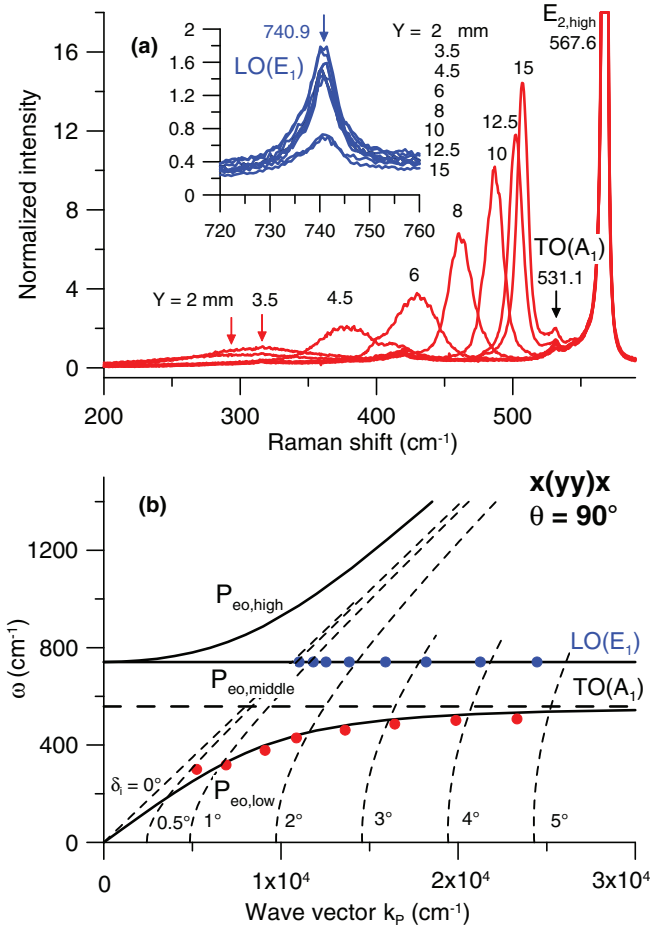

FIG. 8. (Color online) (a) Raman spectra of the extraordinary polariton, $\theta = 90^\circ$, $x(yy)x$. Near-forward scattering in direction x, scattering in the (x,y) plane, polarization parallel $y(y)$ of the incident (scattered) light vectors. The parameter Y indicates the position of the entrance window for the scattered light on the screen (1), $Z = 0$. The inset shows the LO(E_1) phonon at fixed spectral position. (b) Dispersion of the extraordinary polariton branches for $\theta = 90^\circ$ as a function of the polariton wave vector [solutions of Eq. (14)]. The dashed curves [solutions of Eq. (B2)] show possible (ω, k_P) values for scattering angles δ_i inside the crystal (see Fig. 5).

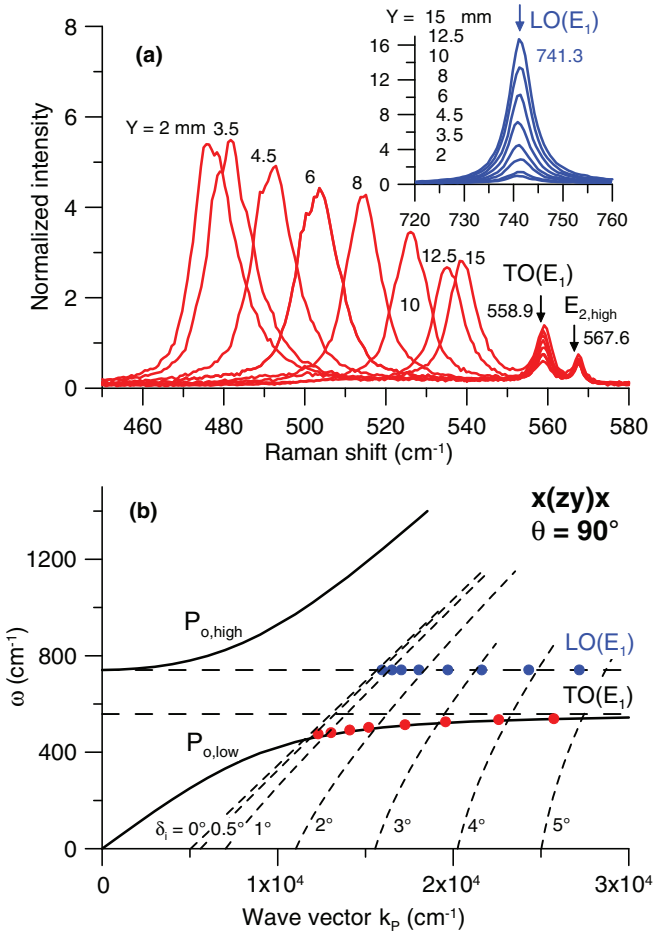

FIG. 9. (Color online) (a) Raman spectra of the ordinary polariton, $\theta = 90^\circ$, $x(zy)x$. Near-forward scattering in direction x, scattering in the (x,y) plane, polarization parallel $z(y)$ of the incident (scattered) light vectors. The parameter Y indicates the position of the entrance window for the scattered light on the screen (1), $Z = 0$. The inset shows the LO(E_1) phonon at fixed spectral position. (b) Dispersion of the ordinary polariton branches for $\theta = 90^\circ$ as a function of the polariton wave vector [solutions of Eq. (11)]. The dashed curves [solutions of Eq. (B2)] show possible $(\omega, \vec{k}_P)$ values for scattering angles δ_i inside the crystal (see Fig. 5).

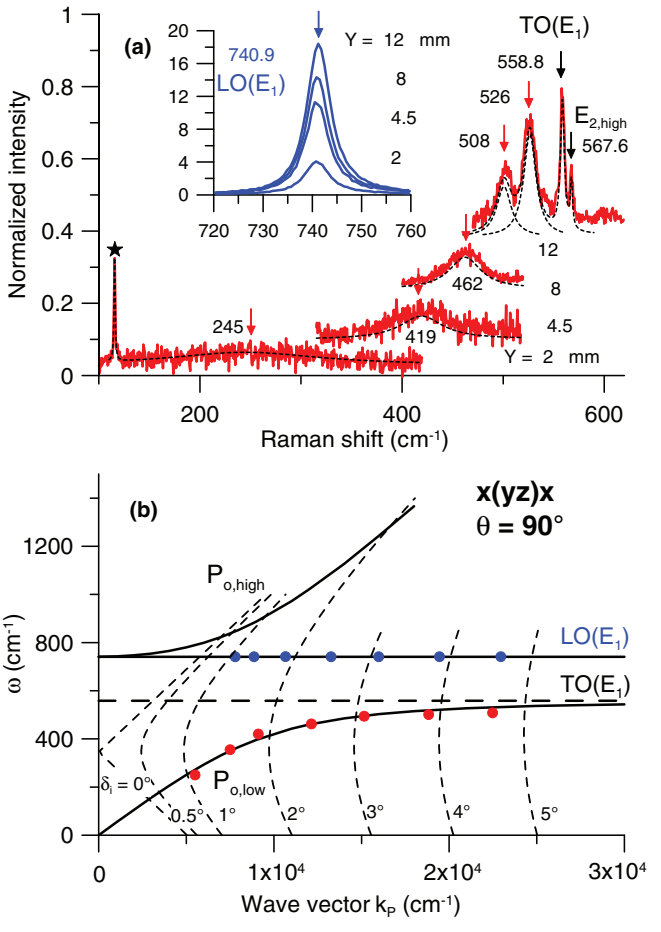

FIG. 10. (Color online) (a) Raman spectra of the ordinary polariton, $\theta = 90^\circ$, $x(yz)x$. Near-forward scattering in direction x, scattering in the (x,y) plane, polarization parallel $y(z)$ of the incident (scattered) light vectors. The parameter Y indicates the position of the entrance window for the scattered light on the screen (1), $Z = 0$. The inset shows the LO(E_1) phonon at fixed spectral position. (b) Dispersion of the ordinary polariton branches for $\theta = 90^\circ$ as a function of the polariton wave vector [solutions of Eq. (11)]. The dashed curves [solutions of Eq. (B2)] show possible $(\omega, \vec{k}_P)$ values for scattering angles δ_i inside the crystal (see Fig. 5).

Figures 7–10 show the near-forward Raman scattering spectra and the dispersion of the polaritons depending on the polariton wave vector for scattering in the (x,y) plane ($\theta = 90^\circ$). The intensities of the Raman spectra were normalized with respect to the intensity of the $E_{2,high}$ Raman mode at 567.6 cm^{-1}, which is allowed in the configuration $x(yy)x$. This nonpolar phonon is connected with lattice displacements parallel to the (x,y) plane and is not influenced by the electric field. Its intensity does not depend on the parameter Y displayed in Figs. 7–10. The polariton Raman bands are shifted towards lower frequencies with decreasing parameter Y. Small values of $Y \approx 2$ mm could be realized. This corresponds to an angle $\delta_i \approx 0.5^\circ$ between the scattered light beam and the x axis. The exciting laser beam passing the crystal was blocked off in the center of the screen in order to avoid entrance of laser light in the spectrometer. The overlay of the scattered light with exciting laser light limits the parameter at small Y values.

Besides the polariton Raman bands small Raman bands at fixed frequencies can be observed, in the Raman spectra of the extraordinary polaritons, the TO(A_1) phonons at 531.1 cm^{-1} and in the Raman spectra of the ordinary polaritons, the TO(E_1) phonon at 558.9 cm^{-1} as well as weak bands of the (very strong) $E_{2,high}$ phonon. Their origin is due to some scattered light that stems from a 180°-backscattering process of phonons with wave vectors of about 6×10^5 cm^{-1} overlaying the near-forward scattering. Part of the incident laser beam is reflected inside the crystal and gives rise to these weak bands, which could be minimized by careful adjustment. Figures 7(a)–10(a) show insets with the measured LO phonons with symmetry E_1 and location at about 741 cm^{-1} in accordance with scattering in the (x,y) plane. The stable position of the measured LO phonon indicates that the scattering occurs in the (x,y) plane ($\theta = 90^\circ$).

The dispersion of the polariton modes is shown in Figs. 7(b)–10(b). The curves $PO_{eo,low}$, $PO_{eo,middle}$, and $PO_{eo,high}$

in Figs. 7(b) and 8(b) for the extraordinary polariton modes are solutions of Eq. (14) and the curves $PO_{o,low}$ and $PO_{o,high}$ in Figs. 9(b) and 10(b) are solutions of Eq. (11). The dashed curves show solutions of Eqs. (32) and (33) for scattering angles δ_i inside the crystal, with combinations of values (ω) and (k_P), allowed due to energy and momentum conservation. The intersections with the theoretical dispersion curves yield the allowed polaritons.

The smaller the angle δ_i, the broader the Raman bands since the slope of the curve becomes steeper. The small bands at 317, 410, and 420 cm^{-1} are acoustic overtones of the second-order Raman spectra.[53] The dashed curves in Fig. 10 illustrate that only the configuration $x(yz)x$ allows one to observe photonlike polaritons on the branch $PO_{o,high}$ in principle. However, for this scattering configuration, the scattering intensity is more than one order smaller than for the other configurations. Further, the slope of this branch rises steeply with increasing δ_i, which increases the half-width of

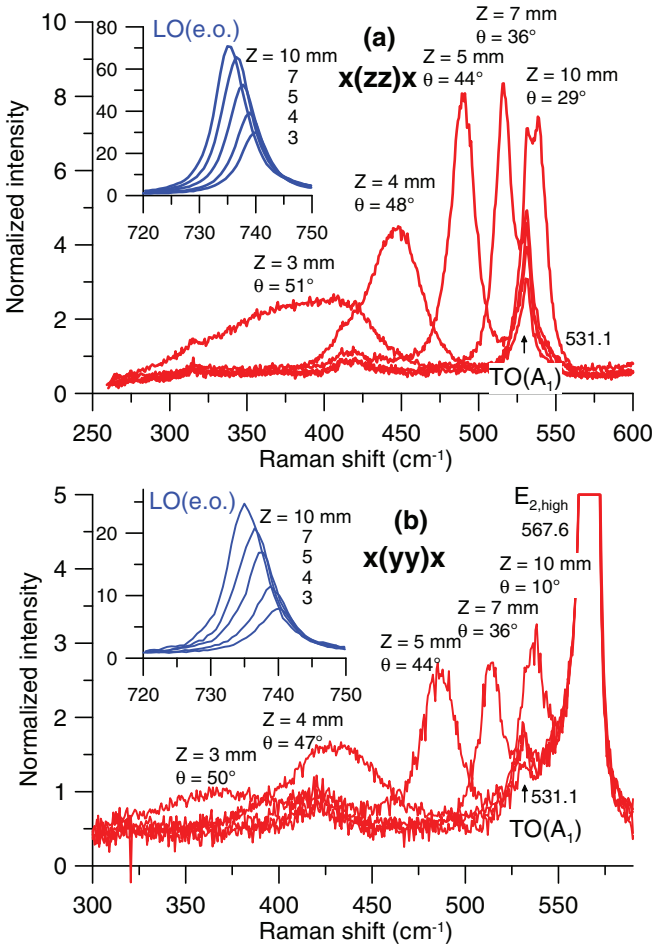

FIG. 11. (Color online) Raman spectra of the extraordinary polariton, near-forward scattering in the (x,z) plane. The parameter Z indicates the position of the entrance window for the scattered light on the screen (1), $Y = 0$. θ is the corresponding angle between the polariton wave vector and the z axis. The two insets show that the position of the LO phonon is shifted owing to the variation of θ (see Fig. 4). The upper panel shows the spectra taken with polarization $z(z)$ of the electric field vector of the incident (scattered) light, the spectra in the lower panel are measured with polarization $y(y)$.

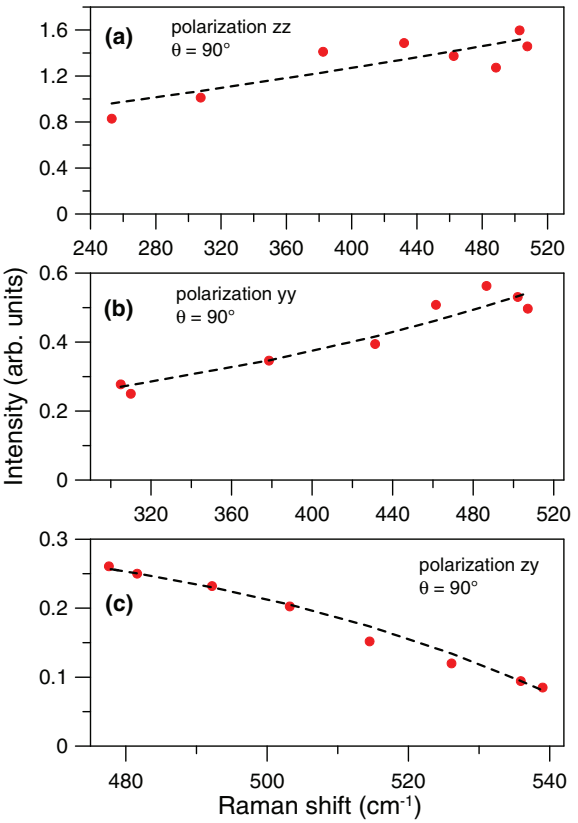

FIG. 12. (Color online) Raman intensity of the polaritons observed in near-forward scattering geometry in the (x,y) plane as function of the Raman shift. (a) Extraordinary polariton, polarization (zz). (b) Extraordinary polariton, polarization (yy). (c) Ordinary polariton, polarization (zy). The circles show experimentally obtained values. The intensity was normalized referring to the Raman intensity of the $E_{2,high}$ phonon measured in polarization (yy). The dashed curves were calculated by Eq. (26).

the expected band. Therefore, despite careful search, we were not able to detect this branch. Figure 11 shows Raman spectra of the extraordinary polariton with near-forward scattering in the (x,z) plane. The parameter Z indicates the position on the screen in vertical direction ($Y = 0$). Figure 11(a) displays spectra with polarization (zz) and Fig. 11(b) with polarization (yy) of the electric field vectors of the incident and scattered light. The intensities of the Raman spectra were normalized with respect to the intensity of the nonpolar $E_{2,high}$ phonon. The intensity of the $E_{2,high}$ phonon is (nearly) independent on the parameter Z in the considered Z range. Depending on the parameter Z, the polariton wave vectors include different angles θ with the z axis. Each Raman spectrum corresponds to different dispersion curves (see Fig. 3). Therefore we omitted the corresponding dispersion curves.

The circles in Fig. 12 give the Raman intensities of the polariton spectra shown in Figs. 7(a)–9(a) for scattering in the (x,y) plane ($\theta = 90°$). The polaritons in the (yz) polarization exhibit only weak scattering intensities. Therefore they were not included in the figure. The intensities shown are the areas beneath the polariton bands normalized to the $E_{2,high}$ Raman mode, which is allowed in the (yy) polarization. The dashed curves were calculated according to Eq. (26) in Sec. II E. The

experimentally obtained intensities show an overall excellent agreement with the theoretical values.

V. CONCLUSION

In this study, Raman scattering of phonon polaritons in uniaxial crystals of wurtzite-type was investigated. The dispersion and the Raman scattering efficiency of the ordinary and extraordinary polaritons were discussed in detail. Starting with the Born-Huang and the Maxwell equations, expressions for the Raman scattering intensity were derived for arbitrary directions of the polaritons in the crystal. In the limit of large wave-vector magnitudes, the equations describe the behavior of the polar phonons. An experimental setup is described that enables measurements of polaritons of defined E_1 and A_1 symmetry depending on their wave vector. Near-forward Raman scattering measurements with angles between laser and scattered light beams down to about 0.5° were possible.

Polariton spectra of α-GaN were measured for different scattering geometries and polarizations. The experimental results are in accordance with the theoretical derivations. Although the birefringence for light in the optical range is only small, strong differences between the polariton Raman spectra in the near-forward configurations $x(zy)x$ and $x(yz)x$ occur. The observation of the photonlike polariton branch should be possible, in principle, in the $x(yz)x$ configuration but escaped detection due to weak Raman signals.

ACKNOWLEDGMENTS

The authors gratefully acknowledge the fruitful cooperation with G. Leibiger and F. Habel (Freiberger Compound Materials GmbH), especially in providing high-quality GaN specimens as well as supporting the sample preparation. This work was performed within the Cluster of Excellence "Structure Design of Novel High-Performance Materials via Atomic Design and Defect Engineering (ADDE)" which is financially supported by the European Union (European regional development fund) and by the Ministry of Science and Art of Saxony (SMWK).

APPENDIX A: BASIC EQUATIONS

The coefficients B in Eqs. (3) and (4) can be correlated with measurable macroscopic parameters (see, for instance, Ref. 30): for transverse phonons in the principal directions with $c^2k^2/\omega^2 \gg 1$, it can be seen that

$$\begin{aligned} B^{11}_{\mathrm{o}\perp} &= B^{11}_{\mathrm{e}\perp} = -\omega^2_{\mathrm{T}\perp}, \\ B^{11}_{\mathrm{e}\parallel} &= -\omega^2_{\mathrm{T}\parallel}. \end{aligned} \tag{A1}$$

For large frequencies ω, the amplitudes of the normal coordinates $Q_{\mathrm{o}\perp}$, $Q_{\mathrm{e}\perp}$, and $Q_{\mathrm{e}\parallel}$ vanish, and we receive from $P_{\mathrm{o}\perp} = B^{22}_{\mathrm{o}\perp}E_{\mathrm{o}\perp} = \varepsilon_0(\varepsilon_{\infty\perp} - 1)E_{\mathrm{o}\perp}$, $P_{\mathrm{e}\perp} = B^{22}_{\mathrm{e}\perp}E_{\mathrm{e}\perp} = \varepsilon_0(\varepsilon_{\infty\perp} - 1)E_{\mathrm{e}\perp}$, and $P_{\mathrm{e}\parallel} = B^{22}_{\mathrm{e}\parallel}E_{\mathrm{e}\parallel} = \varepsilon_0(\varepsilon_{\infty\parallel} - 1)E_{\mathrm{e}\parallel}$ the following:

$$\begin{aligned} B^{22}_{\mathrm{o}\perp} &= B^{22}_{\mathrm{e}\perp} = b_\perp = \varepsilon_0(\varepsilon_{\infty\perp} - 1), \\ B^{22}_{\mathrm{e}\parallel} &= b_\parallel = \varepsilon_0(\varepsilon_{\infty\parallel} - 1). \end{aligned} \tag{A2}$$

In the static case ($\omega = 0$), we obtain for the ordinary modes from $Q_{\mathrm{o}\perp} = -(B^{12}_{\mathrm{o}\perp}/B^{11}_{\mathrm{o}\perp})E_{\mathrm{o}\perp}$ and $P_{o\perp} = [-(B^{12}_{o\perp}B^{21}_{o\perp}/B^{11}_{\mathrm{o}\perp}) + B^{22}_{\mathrm{o}\perp}]E_{\mathrm{o}\perp}$, analog equations for the extraordinary modes, and with Eqs. (A1) and (A2),

$$\begin{aligned} B^{12}_{\mathrm{o}\perp} &= B^{21}_{\mathrm{o}\perp} = B^{12}_{\mathrm{e}\perp} = B^{21}_{\mathrm{e}\perp} = a_\perp \\ &= \omega_{\mathrm{T}\perp}\sqrt{\varepsilon_0(\varepsilon_{\mathrm{s}\perp} - \varepsilon_{\infty\perp})} = \sqrt{\varepsilon_0\varepsilon_{\infty\perp}\left(\omega^2_{\mathrm{L}\perp} - \omega^2_{\mathrm{T}\perp}\right)}, \\ B^{12}_{\mathrm{e}\parallel} &= B^{21}_{\mathrm{e}\parallel} = a_\parallel \\ &= \omega_{\mathrm{T}\parallel}\sqrt{\varepsilon_0(\varepsilon_{\mathrm{s}\parallel} - \varepsilon_{\infty\parallel})} = \sqrt{\varepsilon_0\varepsilon_{\infty\parallel}\left(\omega^2_{\mathrm{L}\parallel} - \omega^2_{\mathrm{T}\parallel}\right)}. \end{aligned} \tag{A3}$$

$\omega_{\mathrm{T}\perp}$ ($\omega_{\mathrm{T}\parallel}$) indicates the frequency of the transverse phonon propagating in the (x,y) plane (parallel to the z axis). $\omega_{\mathrm{L}\perp}$ ($\omega_{\mathrm{L}\parallel}$) refers to the frequency of the longitudinal phonon propagating in the (x,y) plane (parallel to the z axis). $\varepsilon_{\mathrm{s}\perp}$ ($\varepsilon_{\infty\perp}$) denotes the static (high-frequency) dielectric constant in the (x,y) plane and $\varepsilon_{\mathrm{s}\parallel}$ ($\varepsilon_{\infty\parallel}$) is the static (high-frequency) dielectric constant parallel to the z axis. In Eq. (A3), Lyddane-Sachs-Teller relations were used:

$$\begin{aligned} \frac{\omega^2_{\mathrm{L}\perp}}{\omega^2_{\mathrm{T}\perp}} &= \frac{\varepsilon_{\mathrm{s}\perp}}{\varepsilon_{\infty\perp}}, \\ \frac{\omega^2_{\mathrm{L}\parallel}}{\omega^2_{\mathrm{T}\parallel}} &= \frac{\varepsilon_{\mathrm{s}\parallel}}{\varepsilon_{\infty\parallel}}. \end{aligned} \tag{A4}$$

APPENDIX B:NEAR-FORWARD SCATTERING EQUATIONS

For small scattering angles and $|\vec{k}_{\mathrm{iL}}| \approx |\vec{k}_{\mathrm{iS}}|$, it can be assumed that $\vec{k}_{\mathrm{P}} \perp \vec{k}_{\mathrm{iL}}$. In the case of very small scattering angles, we have to consider that the transferred polariton wave vector has also components in the (x,y) plane. With Eqs. (32) and (33), we obtain the polariton wave vector:

$$\vec{k}_{\mathrm{P}} = \frac{2\pi\, n_{\mathrm{S}}(1 - \omega\lambda_{\mathrm{L}})}{\lambda_{\mathrm{L}}}\left(\frac{1}{1 - \omega\lambda_{\mathrm{L}}}\frac{n_{\mathrm{L}}}{n_{\mathrm{S}}} - \cos\psi_{\mathrm{i}}\cos\delta_{\mathrm{i}},\ -\cos\psi_{\mathrm{i}}\sin\delta_{\mathrm{i}},\ -\sin\psi_{\mathrm{i}}\right). \tag{B1}$$

The magnitude of the polariton wave vector is

$$k_{\mathrm{P}} = 2\pi\sqrt{\frac{1}{\lambda^2_{\mathrm{L}}}\left(n^2_{\mathrm{L}} + n^2_{\mathrm{S}}\right) - n^2_{\mathrm{S}}\omega\left(\frac{2}{\lambda_{\mathrm{L}}} - \omega\right) - 2n_{\mathrm{L}}n_{\mathrm{S}}\frac{1}{\lambda_{\mathrm{L}}}\left(\frac{1}{\lambda_{\mathrm{L}}} - \omega\right)\cos\psi_{\mathrm{i}}\cos\delta_{\mathrm{i}}}. \tag{B2}$$

In this equation, k_P is obtained in cm^{-1} if we express λ_L in cm and the Raman shift ω in cm^{-1}. The angle θ between the polariton wave vector $\vec{k}_P$ and the z axis is defined by

$$\cos\theta = \frac{k_{P,z}}{k_P} = \frac{-2\pi\, n_S(1-\omega\lambda_L)\sin\psi_i}{\lambda_L k_P}. \tag{B3}$$

The angle φ between the polariton wave vector and the x axis is determined by

$$\sin\varphi = \frac{k_{P,y}}{\sqrt{k_P^2 - k_{P,z}^2}}. \tag{B4}$$

In the following, it is assumed that the distance L of the imaging lens and the lens radius R are large in comparison with the lateral size of the crystal and the exciting laser path length within the crystal. Furthermore, R should be small in comparison with L. In our case. L = 80 mm and R = 14 mm. It is appropriate to introduce spherical coordinates $x = r\cos\psi\cos\delta$, $y = r\cos\psi\sin\delta$, and $z = r\sin\psi$. Thus the unit vector $\vec{q}_S(\psi,\delta) = \vec{k}_S(\psi,\delta)/|\vec{k}_S(\psi,\delta)|$ of the scattered light beam outside the crystal can be expressed as

$$\vec{q}_S(\psi,\delta) = (\cos\psi\cos\delta, \cos\psi\sin\delta, \sin\psi), \tag{B5}$$

where ψ denotes the angle between the scattered light vector and the (x,y) plane and δ is the azimuthal angle between the orthogonal projection of the scattered light vector on the (x,y) plane and the x axis (see Fig. 13). The lens center is located at $\psi = \delta = 0^\circ$, a rectangular window in the aperture in front of lens 1 can be described by $\Delta Y\Delta Z = \Delta\psi\Delta\delta L^2/(\cos^2\psi\cos^2\delta) \approx \Delta\psi\Delta\delta L^2$.

Further, the direction of the x axis is oriented perpendicularly to the boundary surface of the crystal. The x axis as well as the scattered light vectors inside and outside the crystal are

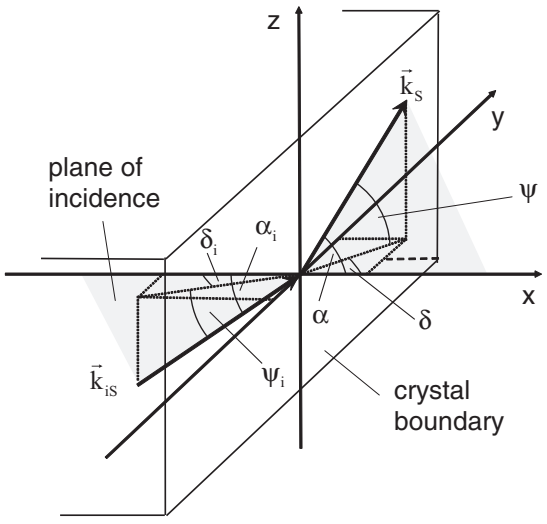

FIG. 13. Refraction of the scattered light at the crystal boundary. Suitably, the angles α and α_i between the unit wave vector of the scattered light (outside and inside the crystal) and the x axis are introduced in order to derive the unit wave vector of the scattered light inside the crystal in dependence on the angles ψ and δ using the law of refraction.

located in the plane of incidence (see Fig. 13). It is convenient to introduce the angles of the unit vectors of the scattered light beams outside ($\vec{q}_S$) and inside the crystal ($\vec{q}_{iS}$) with the axes x, y, and z:

$$\vec{q}_S = (q_{S,x}, q_{S,y}, q_{S,z}) = (\cos\alpha, \cos\beta, \cos\gamma), \tag{B6}$$

$$\vec{q}_{iS} = (q_{iS,x}, q_{iS,y}, q_{iS,z}) = (\cos\alpha_i, \cos\beta_i, \cos\gamma_i). \tag{B7}$$

Using the law of refraction $\sin\alpha_i = \sin\alpha/n_S$, we receive the wave vector (unit vector) of the scattered light inside the crystal in dependence on the angles ψ and δ:

$$\vec{q}_{iS} = \left(\sqrt{1-a}, \frac{-\sqrt{a}}{\sqrt{1+b}}, \frac{\sqrt{ab}}{\sqrt{1+b}}\right), \tag{B8}$$

where $a = (1-\cos^2\psi\,\cos^2\delta)/n_S^2$ and $b = \tan^2\psi/\sin^2\delta$. Depending on the polarization, the refractive index rates as $n_S = n_o$ (ordinary ray) or $n_S = n_{eo}$ (extraordinary ray). It should be noted that Eq. (B8) holds for the ordinary ray but is not exactly valid for the extraordinary ray in all cases. If the plane of incidence does not coincide with the principal plane (defined as a plane containing the wave vector and the z axis), the refracted extraordinary ray no longer lies in the plane of incidence.[54,55] Further, its refractive index depends on the angle ψ. However, in our case, the angles between the scattered light beam and the x axis inside the crystal are small (the largest possible angles are about 4° for scattered light entering the border of the imaging lens), and furthermore, the difference between the two refraction indices n_o and n_{eo} is only small in the case of wurtzitic GaN. Therefore it is justified to also use Eq. (B8) for the extraordinary ray. Thus the transferred polariton wave vector in dependence on the angles ψ and δ is determined by

$$\vec{k}_P(\psi,\delta) = 2\pi\left[\frac{n_L\vec{q}_{iL}}{\lambda_L} - \frac{n_S\vec{q}_{iS}(\psi,\delta)}{\lambda_S}\right]. \tag{B9}$$

The exciting laser beam is directed parallel to the x axis and penetrates perpendicularly the crystal surface without refraction and change of the polarization. For the measurements the following polarizations of the electric field were used: the letters V(H) indicate vertical (horizontal) polarization. As already previously mentioned, the index "i" refers to the inner part of the crystal. The polarization vectors perpendicular to the wave vector of the incident laser beam are $\vec{e}_L^{\,H}(\vec{e}_{iL}^{\,H})$ with horizontal direction parallel to the y axis and $\vec{e}_L^{\,V}(\vec{e}_{iL}^{\,V})$ with vertical direction parallel to the z axis of the laboratory coordinate system:

$$\vec{e}_L^{\,H} = \vec{e}_{iL}^{\,H} = (0,1,0), \tag{B10a}$$

$$\vec{e}_L^{\,V} = \vec{e}_{iL}^{\,V} = (0,0,1). \tag{B10b}$$

A beam of scattered light reaches at $(Y,Z) = (L\tan\delta, L\tan\psi)$ the window on the screen positioned in front of the entrance

lens of the imaging system and then passes parallel to the x axis the analyzer with vertical (V) or horizontal (H) position. The light beam arises from the scattered light leaving the crystal face with a wave vector given by Eq. (B8) and characterized by the two angles ψ and δ. The direction of the beam's wave vector inside the crystal is determined by the refraction law relating to the crystal surface. The polarization vectors of the beam between the crystal and lens 1 are

$$\vec{e}_{\mathrm{S}}^{\,\mathrm{H}} = (-\sin\delta, \cos\delta, 0), \tag{B11a}$$

$$\vec{e}_{\mathrm{S}}^{\,\mathrm{V}} = (-\sin\psi, 0, \cos\psi). \tag{B11b}$$

The polarization vectors of the corresponding scattered beam inside the crystal are

$$\vec{e}_{\mathrm{iS}}^{\,\mathrm{H}} = \frac{\vec{q}_{\mathrm{iS}} \times \vec{e}_z}{|\vec{q}_{\mathrm{iS}} \times \vec{e}_z|} = \frac{1}{\sqrt{q_{\mathrm{iS},x}^2 + q_{\mathrm{iS},y}^2}} (q_{\mathrm{iS},y}, -q_{\mathrm{iS},x}, 0), \tag{B12a}$$

$$\vec{e}_{\mathrm{iS}}^{\,\mathrm{V}} = \vec{e}_{\mathrm{iS}}^{\,\mathrm{H}} \times \vec{q}_{\mathrm{iS}} = \frac{\left(-q_{\mathrm{iS},x} q_{\mathrm{iS},z}, -q_{\mathrm{iS},y} q_{\mathrm{iS},z}, q_{\mathrm{iS},x}^2 + q_{\mathrm{iS},y}^2\right)}{\sqrt{q_{\mathrm{iS},x}^2 + q_{\mathrm{iS},y}^2}}. \tag{B12b}$$

The polarization vectors can be expressed as functions of ψ and δ using Eq. (B8).

*Corresponding author: irmer@physik.tu-freiberg.de

[1] K. Huang, Nature (London) **167**, 779 (1951).
[2] K. Huang, Proc. Roy. Soc. A **208**, 352 (1951).
[3] R. H. Poolman, E. A. Muljarov, and A. L. Ivanov, Phys. Rev. B **81**, 245208/1 (2010).
[4] T. Feurer, J. C. Vaughan, and K. A. Nelson, Science **299**, 374 (2003).
[5] K. Saito, T. Tanabe, Y. Oyama, K. Suto, and J.-i. Nishizawa, J. Appl. Phys. **105**, 063102 (2009).
[6] T. Feurer, N. S. Stoyanov, D. W. Ward, J. C. Vaughan, E. R. Statz, and K. A. Nelson, Annu. Rev. Mater. Res. **37**, 317 (2007).
[7] C. H. Henry and J. J. Hopfield, Phys. Rev. Lett. **15**, 964 (1965).
[8] S. P. S. Porto, B. Tell, and T. C. Damen, Phys. Rev. Lett. **16**, 450 (1966).
[9] C. K. N. Patel and R. E. Slusher, Phys. Rev. Lett. **22**, 282 (1969).
[10] S. Ushioda and J. D. McMullen, Solid State Commun. **11**, 299 (1972).
[11] J. H. Nicola and R. C. C. Leite, Phys. Rev. B **11**, 798 (1975).
[12] J. H. Nicola, J. A. Freitas, and R. C. C. Leite, Solid State Commun. **17**, 1379 (1975).
[13] H. E. Puthoff, R. H. Pantell, B. G. Huth, and M. A. Chacon, J. Appl. Phys. **39**, 2144 (1968).
[14] A. Pinczuk, E. Burstein, and S. Ushioda, Solid State Commun. **7**, 139 (1969).
[15] J. F. Scott, P. A. Fleury, and J. M. Worlock, Phys. Rev. **177**, 1288 (1969).
[16] R. Claus, G. Borstel, and L. Merten, Opt. Commun. **3**, 17 (1971).
[17] E. Burstein, S. Ushioda, and A. Pinczuk, Appl. Phys. Lett. **20**, 230 (1972).
[18] A. D'Andrea, B. Fornari, G. Mattei, M. Pagannone, and M. Scrocco, Phys. Status Solidi B **54**, K131 (1972).
[19] W. S. Otaguro, E. Wiener-Avnear, S. P. S. Porto, and J. Smit, Phys. Rev. B **6**, 3100 (1972).
[20] F. X. Winter and R. Claus, Opt. Commun. **6**, 22 (1972).
[21] F. X. Winter, Phys. Lett. A **40**, 425 (1972).
[22] M. Posledovich, F. X. Winter, G. Borstel, and R. Claus, Phys. Status Solidi B **55**, 711 (1973).
[23] F. X. Winter, E. Wiesendanger, and R. Claus, Phys. Status Solidi B **64**, 95 (1974).
[24] F. X. Winter, E. Wiesendanger, and R. Claus, Phys. Status Solidi B **72**, 189 (1975).
[25] L. A. Kulevsky, Y. N. Polivanov, and S. N. Poluektov, J. Raman Spectrosc. **5**, 269 (1976).
[26] A. S. Barker and R. Loudon, Rev. Mod. Phys. **44**, 18 (1972).
[27] L. Merten, *Atomic Structure and Properties of Solids* (Academic Press, New York, 1972).
[28] L. Merten, *Advances in Solid State Physics XII* (Pergamon Press, New York, 1972).
[29] D. L. Mills and E. Burstein, Rep. Prog. Phys. **37**, 817 (1974).
[30] R. Claus, L. Merten, and J. Brandmüller, *Light Scattering by Phonon-Polaritons*, edited by G. Höhler, Springer Tracts in Modern Physics Vol. 75 (Springer-Verlag, Berlin, 1975).
[31] *Surface Polaritons*, edited by V. M. Agranovich and D. L. Mills (North-Holland Publishing Company, Amsterdam, 1982).
[32] S. S. Ng, T. L. Yoon, Z. Hassan, and H. Abu Hassan, Appl. Phys. Lett. **94**, 241912 (2009).
[33] S. F. Cheah, S. C. Lee, S. S. Ng, F. K. Yam, H. Abu Hassan, and Z. Hassan, Appl. Phys. Lett. **102**, 101601 (2013).
[34] W. L. Faust and C. H. Henry, Phys. Rev. Lett. **17**, 1265 (1966).
[35] M. Cardona, *Light Scattering in Solids II* (Springer-Verlag, Berlin, 1982), p. 19.
[36] M. V. Klein, *Light Scattering in Solids I* (Springer-Verlag, Berlin, 1983), p. 147.
[37] G. Abstreiter, M. Cardona, and A. Pinczuk, *Light Scattering in Solids IV* (Springer-Verlag, Berlin, 1984), p. 5.
[38] G. Irmer, V. V. Toporov, B. H. Bairamov, and J. Monecke, Phys. Status Solidi B **119**, 595 (1983).
[39] H. Morkoc, S. Strite, G. Gao, M. Lin, B. Sverdlov, and M. Burns, J. Appl. Phys. **76**, 1363 (1994).
[40] S. Nakamura, T. Mukai, and M. Senoh, Appl. Phys. Lett. **64**, 1687 (1994).
[41] S. Nakamura, Solid State Commun. **102**, 237 (1997).
[42] I. Akasaki and H. Amano, Jpn. J. Appl. Phys. **36**, 5393 (1997).
[43] J. S. Speck and S. F. Chichibu, MRS Bull. **34**, 304 (2009).
[44] K. Torii, M. Ono, T. Sota, T. Azuhata, S. F. Chichibu, and S. Nakamura, Phys. Rev. B **62**, 10861 (2000).
[45] C. A. Arguello, D. L. Rousseau, and S. P. S. Porto, Phys. Rev. **181**, 1351 (1969).
[46] I. N. Bronshtein, K. A. Semendyayev, G. Musiol, and H. Mühlig, *Handbook of Mathematics* (Springer-Verlag, Berlin, 2007).
[47] H. Poulet, Ann. Phys. (Paris) **10**, 908 (1955).
[48] R. Loudon, Adv. Phys. **13**, 423 (1964).
[49] J. W. D. Johnston, Phys. Rev. B **1**, 3494 (1970).
[50] A. S. J. Barker and M. Ilegems, Phys. Rev. B **7**, 743 (1973).

[51]G. Yu, H. Ishikawa, T. Egawa, T. Soga, J. Watanabe, T. Jimbo, and M. Umeno, Jpn. J. Appl. Phys. **36**, L1029 (1997).
[52]V. Y. Davydov, Y. E. Kitaev, I. N. Goncharuk, A. N. Smirnov, J. Graul, O. Semchinova, D. Uffmann, M. B. Smirnov, A. P. Mirgorodsky, and R. A. Evarestov, Phys. Rev. B **58**, 12899 (1998).
[53]H. Siegle, G. Kaczmarczyk, L. Filippidis, A. P. Litvinchuk, A. Hoffmann, and C. Thomsen, Phys. Rev. B **55**, 7000 (1997).
[54]M. Born and E. Wolf, *Principles of Optics* (Cambridge University Press, Cambridge, 1999).
[55]S. A. Akhmanov and S. Y. Nikitin, *Physical Optics* (Clarendon Press, Oxford, 1997).